# ACCURACY ANALYSIS OF HYPERSPECTRAL IMAGERY CLASSIFICATION USING LEVEL SETS

**John Ball**, Graduate Student
**Dr. Lori M. Bruce**, Associate Professor
Mississippi State University
Mississippi State, MS 39762
jball@ece.msstate.edu
bruce@ece.msstate.edu

## ABSTRACT

Image classification is an important task in the remote sensing field. In a previous study, the authors presented a semi-automated supervised level set-based hyperspectral image segmentation algorithm (LSHSA) (Ball and Bruce, 2005). The LSHSA method used specialized speed functions created using pixel similarity and class discriminator functions. The pixel similarity function was based on an exponential term using three of the data bands with equal contributions from each band. The class discriminator functions had experimentally determined thresholds that were based on the training data, and were used to stop the segmentation at natural boundaries. This procedure is modified by using stepwise Fisher's linear discriminant analysis (FLDA) with a receiver operating characteristics (ROC) decision metric to determine the best bands for class separation. Four new speed functions are proposed and investigated, based on an identity matrix, the covariance matrix, FLDA weighting coefficients, and the Fisher's between-class covariance matrix. A HYDICE 191 band hyperspectral image of the Washington D.C. Mall area is used to validate the algorithm (Ball and Bruce, 2005). The classes segmented are grass, water, trees, paths, shadows and buildings. The results of the proposed algorithm are compared to the results from the previous study using the LSHSA and the maximum likelihood (ML) classifier. The results show that the new method provides better results than the previous LSHSA and ML. The main contribution of this paper is a new best bands-based speed function for segmenting hyperspectral imagery using the level set methodology with improved results over the original LSHSA.

## INTRODUCTION

In a previous study, the authors presented LSHSA (Ball and Bruce, 2005). To our knowledge, this was the first study using level sets to segment hyperspectral imagery. This paper provides a further enhancement of the previous methods for using level sets for semi-automated endmember segmentation in remotely sensed hyperspectral imagery. The paper is organized as follows. First, current methods of dimensionality reduction and hyperspectral image segmentation are discussed. Level set segmentation methods, FLDA and ROC methods are summarized, and the level set discriminator, spectral similarity and speed functions are explained. The band selection and level set segmentation procedures are explained. Finally, the experiments are discussed, and the results analyzed.

## CURRENT METHODS

### Dimensionality Reduction Methods

Hyperspectral data typically have highly correlated bands (Lillesand *et al.*, 2003), and for many processing algorithms, dimensionality reduction (DR) is required since the Hughes phenomenon can cause poor performance for high dimensional data (Duda *et al.*, 2001). DR, also known as best bands analysis (BBA), is a common practice in hyperspectral remote sensing applications (Lillesand *et al.*, 2003). There are many methods for band selection, but all of the algorithms share the common goal of maximizing classifier or segmentation accuracy while keeping only the bands that best discriminate endmembers. Many of the DR methods utilize a discrimination metric such as ROC area under the curve ($A_Z$), Bhattacharyya Distance (BD), Jeffries Matsuhita distance (JMD), etc. Many of these algorithms also use a linear or non-linear transformation in order to analyze and separate the classes. Some of the more common methods are: wavelet analysis; principal components analysis (PCA); independent component analysis (ICA); statistical moment analysis (SMA); kernel-based nonlinear projection (KBNLP); spectral angle mapping (SAM); modified Gram-Schmidt (MGS); linear projection pursuits (PP); canonical analysis (CA); and localized discriminant

bases (LDB).

Bruce, Koger, and Li used wavelet based features and ROC curve based feature selection for classification of pure and mixed pixels. The dataset was a 2151 band dataset taken with Analytical Spectral Devices (ASD) Fieldspec Pro FR spectroradiometer. They achieved from 80% to 95% overall accuracy (Bruce *et al.* 2002). Kaewpijit, Le Moigne, and El-Ghazawi also used wavelet based analysis and found that with the same level of data reduction, that wavelet based methods provided the same or better classification accuracies compared to PCA (Kaewpijit *et al.*, 2003). Li, Bruce and Mathur prove theoretically and experimentally an abundance estimation using a least squares estimation can be improved by using wavelet based analysis and band reduction. They used 2151 band ASD Fieldspec Pro hyperspectral data. The primary advantage of using a wavelet based analysis is the ability to examine multiple bands using the wavelet coefficients (Li *et al.*, 2002). Chang *et al.* presented a joint band selection and decorrelation method, using PCA and classification-based criteria on 210 band HYDICE datasets. They examined minimum variance PCA and maximum SNR PCA, FLDA, and subspace-based projections in conjunction with band prioritization based on eigenanalysis and band decorrelation based on a band divergence criteria. They determined that even with only keeping 10% of the bands, good classification results could be obtained (Chang *et al.*, 1999). Cheriyiadat and Bruce examined PCA for DR and showed that although it is a very popular method, it may yield suboptimal results when the end result is target classification (Cheriyadat and Bruce, 2003). They analyzed synthetic cases and 2151 band hyperspectral data from a Fieldspec Pro spectroradiometer. Du *et al.* used a modified ICA method and PCA for DR and showed that the proposed ICA-based method was superior to PCA for dimensionality reduction of six band multispectral data from a custom Pulnix digital multispectral camera (Du *et al.*, 2003). Du used high order moments SMA analysis, using 158 band AVIRIS images of a volcanic crater. A Neymen-Pearson eigen-thresholding detection theory approach was used to select the number of bands. This was a preliminary study, but the results were promising (Du, 2003).

Gu *et al.* used KBNLP which required three processing steps: subspace partitioning of the data space, kernel PCA based feature extraction, and band selection based on a separability metric. Their results were found to be better than PCA for classification accuracy. The data used were 192 band AVIRIS images and 32 band airborne imaging spectroradiometer for applications (AISA) data (Gu *et al.*, 2002). Kuybeda *et al.* used a modified Gram-Schmidt algorithm that finds the most distant pixels according to an orthogonal complement norm metric and derived a termination procedure for the algorithm. They used a hyperspectral 95 band image (Kuybeda *et al.*, 2004). Lin and Bruce utilized PP to perform band analysis. ROC $A_Z$ and Bhattacharyya distance were metrics used in the band selection. Their results showed that serial parametric projection pursuits (SPPP) provided the best results in distinguishing two weeds from a crop using approximately 2000 band hyperspectral data from an ASD Fieldspec Pro. The accuracies obtained using SPPP were > 95% (Lin and Bruce, 2004). Riedmann and Milton used HYMAP and CASI data and provided an algorithm for band selection which was implemented in IDL/ENVI. It achieved good classification using the ML classifier (above 97% using 2 to 12 bands) (Riedmann and Milton, 2003). Tu *et al.* proposed a two-stage classifier based on a first band reduction stage using CA and a recursive ML (RML) classifier using a 60 band dataset from Purdue University. Their method showed similar performance to ML classification and a considerable speedup in processing time, from 4x to 150x speedup, depending on the final number of bands (Tu *et al.* 1998). Venkataraman *et al.* utilized LDB with decision metrics to distinguish Cogongrass from Johnsongrass, which are two invasive species that look very similar spectrally. Data separation metrics were ROC curve $A_Z$, BD, JMD, and band correlation, and various combinations of these metrics. Data fusion is also performed in the classification stage using multiple classifiers. The data was 2000 band data collected with an ASD Fieldspec Pro. They achieved classification accuracies of 80% – 90% using LDA and qualified majority voting (Venkataraman *et al.* 2005).

## Image Segmentation Methods

There are many different approaches to hyperspectral image segmentation. Some of the more popular methods are maximum likelihood (ML); clustering; kernel-based methods such as support vector machines (SVM), kernel Fisher's discriminant (KFD) analysis, and radial basis neural networks (RBNN); and more recently, active contour (AC) and level set methods.

The ML classification algorithm is the most common method for remote sensing image segmentation. ML uses estimates of each classes mean and covariance to decide the most likely class membership. The method is well understood and implemented in many commercial remote sensing software packages such as ERDAS Imagine, IDL/ENVI and Multispec. Drawbacks of ML classification are that an adequate number of training samples are required, and performance generally degrades as the number of training samples decreases. ML requires inversion of the covariance matrix, which can become ill-conditioned if the number of training samples is inadequate. ML is subject to the Hughes phenomenon (Duda *et al.*, 2001), which means as the data dimensionality increases, the classification accuracy will generally decrease. Also, most ML applications assume a normally distributed dataset, which must be verified (Lillesand *et al.*, 2003).

Clustering is described in (Duda *et al.*, 2001). Typical clustering algorithms use statistical measures to group pixels. Some clustering algorithms require seed point selection by a user and others determine seed points on their own. Clustering can be used as a segmentation method and as an initial method to select training samples, especially when the true number of endmembers in the image is unknown (Lillesand *et al.*, 2003). Kernel-based methods have been employed in the past few years for hyperspectral image classification. Camps-Valls and Bruzonne analyzed several methods including SVM, KFD, RAB, and RBNN. They found that all methods had high output accuracies, and that KFD and SVM had a medium and high robustness to high data dimensionality. The data was AVIRIS data with 16 classes (Camps-Valls and Bruzonne, 2005). Halldorsson *et al.* examined SVM with data fusion using decision boundary feature extraction and nonparametric weighted feature extraction. The class conditional probabilities from each class were used in the decision fusion stage. They found that splitting the data into three independent sources followed by feature extraction from each source and then SVM classification resulted in from 80% to 95% classification accuracy. In general, accuracy increased as the number of features grew (Halldorsson *et al.* 2004).

There has been extensive research and development into level set and active contour image segmentation in general, and this method is just beginning to be used in multispectral and hyperspectral image analysis. The methods typically use PDE-based solutions with functions that control the segmentation by expanding it outwards and penalty functions that may control the curvature or attempt to stop the segmentation growth at natural boundaries (Osher *et al.*, 2003) and (Suri *et al.*, 2002). Numerous examples of examples of level set-based edge detection, segmentation, and medical image analysis are given in (Osher *et al.*, 2003) and (Suri *et al.*, 2002). Suri employed level sets for brain segmentation (Sumengen *et al.*, 2001). Krissian, Ellsmere, Vosburgh, Kikinis, and Westin used level sets for segmentation of the aorta in 3D ultrasound images (Krissian *et al.*, 2001). Sumengen, Manjunath and Kenney used level sets to segment 2D Cardiac Magnetic Resonance Images (MRI) and 3D prostrate MRI (Sumengen *et al.*, 2001). In multispectral and hyperspectral image analysis, Keaton and Brokish used level sets to segment roads in pan sharpened IKONOS multispectral images (Keaton and Brokish, 2002), Dell'Acqua, Gamba and Prevedini extracted and tracked moving clouds in GOES and Meteosat IR satellite image sequences (Gamba *et al.*, 2000), and Harper and Reilly used level sets to segment faces in RGB video (Harper and Reilly, 2000). Lee, Snyder and Wang used active contours to segment real and synthetic RGB images. Their method used the level set methodology and used a multivariate mixture density model to analyze dissimilarities between regions in the image (Lee *et al.* 2005). Ball and Bruce segmented hyperspectral multi-class images with level sets. The data used was 191 band HYDICE images and compared the results for a six class problem to a ML classification. Both algorithms performance was similar (Ball and Bruce, 2005).

## Level Sets Methods

For 2D image segmentation, the level set boundary is the zero level set of a 3D implicit function . The level set methodology tracks the motion of the zero level set boundary according to forces acting normally to the zero level set curve. In the level set methodology, 2D level sets can be visualized as the level surfaces of a 3D function, and a simple partial differential equation (PDE) controls the changes to the level surface (Sethian, 1999). In order to achieve fast processing of the level set propagation, the function is defined on a discrete set of points in 2D space (Sethian, 1999). The level set equation for front propagation with a 2D speed function, $F(x,y)$, acting normal to the level set curve, is given by the PDE $\phi_t + \mathbf{F}|\nabla\phi| = 0$, where $\phi_t$ is the partial derivative of $\phi$ with respect to time, $\nabla\phi(x,y)$ is the gradient of $\phi$ and $|.|$ is the magnitude operator (Sethian, 1999). The level set evolves according to the speed function, ***F***, and it will continue to propagate as long as the speed function is positive. Therefore, when level sets are used for image segmentation, the segmentation problem becomes one of determining the appropriate speed function and initializing the implicit function zero level set points at the seed points. The speed function can be created using two opposing forces: one to grow the segmentation, and the other to stop the segmentation at natural boundaries, such as the distinct line between a body of water and grass on the shore. For the interested reader, the basics of the level set methodology are found in Sethian's book (Sethian, 1999), and many diverse applications and methods are discussed in (Sethian, 1999), (Suri *et al.*, 2002) and (Osher *et al.*, 2003).

## FLDA and ROC $A_Z$

**FLDA** FLDA is a method commonly used for data dimensionality reduction (Fukanaga, 1990). The basic idea is that FLDA will create a linear transformation that simultaneously maximizes the between class variance and minimizes the within class variance, thus separating the classes as much as possible. FLDA assumes normally distributed data and provides a method to determine an optimal separation of the feature vectors for a *C* class problem into a separated feature vector with dimensionality *C*-1. Therefore, for a two class problem, FLDA returns a scalar feature. FLDA

maximizes the functional $J(w) = (w^T S_B w)(w^T S_W w)^{-1}$, where $S_B$ and $S_W$ are the between-class and within-class scatter matrices, respectively (Fukanaga, 1990), (Welling, 2006). For a two class problem, $S_B$ is

$$S_B = (m_T - m_N)(m_T - m_N)^T \ , \tag{1}$$

where $m_T$ and $m_N$ are the mean vectors of the target and non-target class, respectively (Welling, 2006). FLDA generates an optimal solution (a set of weights applied to the data) that will best separate the target and non-target distributions (for a two class problem). It has been shown (Welling, 2006) that the optimal solution weighting matrix, $w_{OPT}$, is

$$w_{OPT} = S_B^{-1/2} v \tag{2}$$

where $S_B^{-1/2}$ satisfies $S_B = S_B^{1/2} S_B^{1/2}$, and $v = S_B^{1/2} w$. Both $w$ and $v$ must also satisfy $S_W^{-1} S_B w = \lambda w$. The solution to equation (2) is the eigenvector $w$ corresponding to the largest eigenvalue, $\lambda$ (Welling, 2006).

**ROC $A_Z$** ROC $A_Z$ (the area under the ROC curve), varies from 0.5 for the worst case scenario, where there is no data separating power, to 1.0 in the best case, where there is perfect data separating power. Higher values of $A_Z$ generally indicate increasing data separation capability of the system (Hanley and McNeil, 1982). An exhaustive search of all band combinations is intractable for hyperspectral images due to the large image size and number of bands. SLDA provides a good compromise in a search for a near optimal subset of bands.

## Level Set Segmentation

This section describes the hyperspectral level set segmentation methodology used in (Ball and Bruce, 2005).

***Class Discrimination Functions.*** Class discrimination functions, $\mathbf{D}_c$, for a class *c*, are 2D functions which attempt to distinguish the different classes based on the unique spectral characteristics of each class. First, vegetation (grass, trees) and non-vegetation (paths, buildings, shadows, and water) are separated. To further discriminate the vegetation classes (trees and grass), a tree-discriminator is employed, which is based on the tree and grass training signatures. The other classes are discriminated in a similar manner. The Normalized Difference Vegetation Index (NDVI) is used to separate vegetation from non-vegetation. NDVI is the most common method of differentiating vegetation from non vegetation (Lillesand *et al.*, 2003). Once vegetation and non-vegetation are separated by the NDVI discriminator, the vegetation classes need separation. Note that all discriminator functions are evaluated for every pixel in the image. The discriminator functions used in this study are exactly the same as those listed in the original level set segmentation methodology (Ball and Bruce, 2005).

***Speed Function.*** The speed function should allow the level set to propagate the segmentation if the boundary pixel signatures are similar to the seed signature. For each class, the seed pixel will be set to the mean value of the training signatures. The spectral similarity to each pixel is calculated using a set of best bands for each class. The level set must be stopped at proper boundaries, which is accomplished by multiplying the similarity function by the class discrimination function at each image pixel. These two functions are discussed next.

***Spectral Similarity Function.*** The spectral similarity function compares the similarity of each pixel to a given seed pixel signature. In (Keaton and Brokish, 2002), Keaton and Brokish define a spectral similarity function, $\mathbf{S}_c$ for a class *c*. Let *c* be the class number, $\boldsymbol{B}$ be a subset of the image bands, $\mathbf{s}_c$ be a vector containing the normalized mean value of a set of seed pixels for class *c*, $I(x, y)$ be the normalized signature of the pixel in the image at location (*x*,*y*), and $\mathbf{D}_c$ be the class discriminator function defined in (Ball and Bruce, 2005). The image and seed pixel normalization is performed by dividing the signature by the largest DN value for all pixels and all bands in the image. Then the spectral similarity function, based on the band subset $\boldsymbol{B}$, is given by

$$\mathbf{S}_c(x,y) = \exp\left\{-\frac{1}{2}\left(\mathbf{I}(x,y) - \mathbf{s}_c\right)\Big|_{\mathbf{B}} \boldsymbol{\Sigma} \left(\mathbf{I}(x,y) - \mathbf{s}_c\right)\Big|_{\mathbf{B}}^{\mathbf{T}}\right\} \ , \tag{3}$$

where the matrix transpose operator is $\mathbf{T}$, and $\mathbf{x}|_{\mathbf{B}}$ means the argument $\boldsymbol{x}$ is evaluated only for the bands in $\boldsymbol{B}$. Note that in (Keaton and Brokish, 2002), $\boldsymbol{\Sigma}$ was originally defined as $\boldsymbol{\Sigma}^{-1}$. Equation (3) is evaluated for each pixel (*x*,*y*) in the image and for each class $c = 1, \ldots, C$, where *C* is the total number of classes. Thus if there are $C = 6$ classes, then there will be six speed functions generated. For a given class *c*, the pixels that most closely match the seed pixel signature

will have larger values of $\mathbf{S}_c$, while pixels that don't match closely will have small values of $\mathbf{S}_c$. The level set algorithm will not allow the segmentation area to propagate to the pixels where $\mathbf{S}_c$ has a near zero value.

## METHODOLOGY

Keaton and Brokish suggest that $\mathbf{\Sigma}$ can be altered based on the image statistics, but do not provide a method for performing this step (Keaton and Brokish, 2002). The focus of this study is centered on investigating the differences in accuracy by using different matrices $\mathbf{\Sigma}$. The following four methods are proposed: (method 1) an appropriate identity matrix; (method 2) the inverse of the covariance matrix of the training data; (method 3) the inverse of the between class covariance matrix from FLDA analysis; and (method 4) a matrix composed from the FLDA weight coefficients. Method 5 uses a 3 x 3 identity matrix, and method 6 is based on ML classification. These methods are summarized in Table 1, below. Methods 1-4 are the new methods examined, and methods 5 and 6 are the original methods described in (Ball and Bruce, 2005), and are used for baseline comparison purposes.

**Table 1. Description of experimental methods.**

| Method Number | Classification Method | Description | Bands Used |
|---|---|---|---|
| Method 1 | Level Set | Identity matrix of appropriate size based on selected bands. | Best bands selected. |
| Method 2 | Level Set | Covariance matrix of training data. | Best bands selected. |
| Method 3 | Level Set | FLDA between-class covariance matrix – reference equation (1). | Best bands selected. |
| Method 4 | Level Set | Matrix of FLDA weights – reference equation (4). | Best bands selected. |
| Method 5 | Level Set | 3x3 identity matrix. This method provides a baseline. | Bands 36, 52 and 63. |
| Method 6 | ML | This method provides a baseline. | Bands 36, 52 and 63. |

Method 4 uses the FLDA weights, and $\mathbf{\Sigma}$ is calculated as follows. Assume that there are *b* bands selected. If $\boldsymbol{w}$ is the vector of FLDA weights from the band selection algorithm, with $\boldsymbol{w} = [w_1 \cdots w_b]$, then $\mathbf{\Sigma}$ is given by the following equation for $i, j \in \{1, \cdots, b\}$ :

$$\mathbf{\Sigma}_{i,j} = \begin{cases} w_i & i = j \\ 0 & otherwise \end{cases} . \tag{4}$$

For this study, equation (3) is modified by changing the matrix $\mathbf{\Sigma}$ and using a new scalar multiplier based on the method. Let the best bands selected for class *c* be $\boldsymbol{B}_c = \{b_1, \ldots, b_{N_c}\}$. The speed function $\tilde{\mathbf{S}}_{k,c}$ for method *k* and class *c* is

$$\tilde{\mathbf{S}}_{k,c}(x,y) = \mathbf{D}_c(x,y) \cdot \exp\left\{-\alpha_k \left[\left(\mathbf{I}(x,y) - \mathbf{s}_c\right)\Big|_{\mathbf{B}_{c,k}}\right] \mathbf{\Sigma}_{k,c} \left[\left(\mathbf{I}(x,y) - \mathbf{s}_c\right)\Big|_{\mathbf{B}_{c,k}}\right]^{\mathbf{T}}\right\}, \tag{5}$$

where $k \in \{1, \cdots, 5\}$ is the method, *c* is the class number, *C* is the total number of classes, $\mathbf{s}_m$ is the normalized mean value of the signature of class *c* training pixels, $\mathbf{\Sigma}_{k,c}$ is the weight matrix for method *k* and target class *c*, $\alpha_k$ is a weighting constant, and $\mathbf{D}_c$ is the class discriminator function defined in (Ball and Bruce, 2005). The notation **T** means the matrix transpose, and $\boldsymbol{x}|_{\boldsymbol{B}_c}$ means the argument $\boldsymbol{x}$ is evaluated only for the bands in $\boldsymbol{B}_c$. The weighting constant $\alpha_k$ was experimentally determined. The final level set speed function for each class *c* is given by the following equation, which is evaluated at all points (*x, y*) in the image:

$$\tilde{\mathbf{F}}_{k,c}(x,y) = \mathbf{D}_c(x,y) \cdot \tilde{\mathbf{S}}_{k,c}(x,y) . \tag{6}$$

***Level Set Multiple Class Segmentation.*** To discriminate classes, the hyperspectral properties of each class are exploited (Lillesand *et al.*, 2003), (Landgrebe, 2003). There are several methods of segmenting images into multiple

classes using level sets: one method is to let each class have a unique disjoint level set and have rules prohibiting overlap (Brox and Weickert, 2004); another method is to use a keep-out region which prohibits a propagating front from moving into the region (Mitchell 2005). This study uses a method in which each class will be sequentially segmented, and each class can overwrite the previous classes' segmentation. The image is segmented in the following order: water, paths, grass, trees, buildings, and then shadows.

## Band Selection Algorithm

Stepwise LDA (SLDA) using FLDA, forward selection, and backwards rejection will be used for band selection, with ROC curve area $A_Z$ as the decision metric. The following section describes the band selection algorithm, which is similar to the algorithm discussed in (Venkataraman, 2005), with the addition of backwards rejection. The forward selection procedure starts by calculating $A_Z$ values for each band separately, using one class as the target and all others as the non-target. The $A_Z$ values are then sorted in descending order. The band with the highest $A_Z$ value gets placed into a feature vector and ROC area is $A_{Z1} = A_Z$. The second best band is then appended to the feature vector and $A_{Z2}$ is computed. The second best band is only retained if $A_{Z2} > A_{Z1}$. Then the third best band is then appended to the feature vector and $A_{Z3}$ is computed. The third best band is only retained if $A_{Z3} > A_{Z2}$. This process is continued until all bands are examined, or until the maximum number of bands allowed is reached. The maximum number of bands is determined by the minimum number of training signatures for a class (Fukanaga, 1990). As a rule of thumb, for every ten training signatures, one feature can be added. Therefore to keep five bands, there needs to be at least 50 training signatures for each class.

Next, backwards rejection is then performed. Assume at this stage that there are $b$ bands selected in the feature vector and the best ROC area is $A_{Z\_BEST}$. If $b > 1$, then the first feature is removed and the ROC area $A_{Z1'}$ is calculated. If $A_{Z1'} > A_{Z\_BEST}$ , then the first feature is removed and $A_{Z\_BEST}$ is set to $A_{Z1'}$. This process continues until all bands have been removed and the ROC area recalculated. At the end of the procedure, there is a feature vector which contains the set of selected bands, the best $A_Z$ value found, and the weighting coefficients (reference equation (1) ).

## Segmentation Methods

Four different level set segmentation methods will be examined (methods 1-4), and the results compared to the original level set segmentation method (method 5) and ML (method 6). Methods 5 and 6 are the same as proposed in (Ball and Bruce, 2005) and use the original three bands: 36, 52, and 63. The following sections discuss the various segmentation methods. The methods summarized in Table 1 will be used to examine the effects of different matrices $\boldsymbol{\Sigma}$ in equation (5) on classification accuracy.

## Segmentation Algorithm

The following algorithm is used to perform the level set segmentation. The discriminator functions used in (Ball and Bruce, 2005) did not allow the level sets to propagate to all pixels in the image, and therefore pixels were left unclassified. For this study, since the discriminator functions were not changed from the original study, all unlabeled pixels will be classified as grass, since this is the most prevalent endmember. The segmentation algorithm is shown in Figure 1 below.

```
Begin LSHSA Algorithm

  Set the initial segmentation to all pixels unlabeled.
  Perform band selection using SLDA (for k=5, use bands shown in Table 1).
  For each class c=1 to 6
    Calculate the discriminator functions D_c .
    For each method k=1 to 5
      Calculate  Σ_{k,c}  according to the methods in Table 1.
      Calculate the speed function using equations (5) and (6).
      Using the level set method, segment class c from the image.
    End For
  End For
  Force unlabeled pixels to grass.

End LSHSA Algorithm
```

**Figure 1.** LSHSA algorithm for methods 1-5 (Reference Table 1).

## General Details

The work in this study is done using MATLAB, except for selection of training signatures, which is done in ERDAS Imagine. MATLAB was Matlab student version 7.0.1.15 (R14) Service Pack 1. The ERDAS Imagine software suite is version 8.6, dated November 12, 2002, from Leica Geosystems Inc. (http:gis.leica-geosystems.com/ product_units/geographic_imaging/, 2005). The level set code used is the Matlab Toolbox for Level Sets version 1.1 beta, dated March 6, 2005, which can be downloaded without charge from the author's website (Mitchell, 2005).

To select training pixels, areas of interest are created using the region growing functionality functions in Erdas Imagine (http:gis.leica-geosystems.com/product_units/geographic_imaging/, 2005), which will generate statistically homogeneous sets of pixels for each class. Validation points were chosen by hand for each class. The classification results are compared to the hand labeled ground truth data by using a confusion matrix and the user's, producer's and overall accuracies. The confusion matrix compares the classification results to known ground truth data on a class by class basis. Producer's accuracy describes how well pixels of a given class are classified, and user's accuracy is a measure of the probability that a classified pixel matches what class is actually on the ground (Lillesand *et al.*, 2003), (Congalton, 1998).

## DATA

The hyperspectral data is a 191 band raw digital number (DN) hyperspectral image of the Washington D.C. Mall area in the U.S.A. The D.C. Mall image is provided on a compact disk which accompanies the book by Landgrebe (Landgrebe, 2003). The D.C. Mall image was taken by the Hyperspectral Digital Imagery Collection Experiment (HYDICE) sensor on August 23, 1995. For more information, reference (http://www.lars.purdue.edu/home/image_ data/ hydice_dc_wavelengths.html, 2005). HYDICE is a push broom aircraft sensor system which operates in the spectral range of 400 to 2500 nm and provides 320 columns across-track by 210 spectral bands with approximately 10 nm spectral resolution (http://aviris.jpl.nasa.gov/, 2005). After several noisy bands were removed, the final image has 191 spectral bands. In this paper, the term band refers to the image band, which is not necessarily the sensor band, since some of the sensor bands were eliminated. All band wavelengths are the band center wavelengths. A smaller sub-image was created from the larger original image, which has dimensions of 129 by 235. The image is shown in Figure 2 (a) as a false color images created from bands 63, 52, and 36 (red, green, and blue, respectively), and is the DC_1 image in (Ball and Bruce, 2005).

## RESULTS

The segmentation algorithm in Figure 1 was applied to the test image. The first step was to select the best bands by comparing each class to all of the other classes using SLDA. Table 2 shows the resulting $\boldsymbol{A_Z}$ values and bands selected. Note that in the cases of shadows and trees, only one band was selected. All endmembers had $\boldsymbol{A_Z}$ values higher than 0.9 except for paths and trees. Tree signatures can easily look like grass signatures, since the trees had leaves at the time of the image. Figure 2(a) shows plots of the $\boldsymbol{A_Z}$ values vs. band number from best bands analysis for the grass endmember, and Figure 2(b) shows plots of the PDF of the signature values after transformation using the FLDA weights from equation (2). Notice how the grass signatures are clustered on the right side of the feature space, while the water, buildings, and paths endmembers are mostly well separated, as expected. There is a small overlap of paths and grass, and trees and grass. The path and grass overlap could be due to a grassy area that is trodden down, which appears to the sensor as a path-like area. The trees and grass have very similar looking spectral characteristics, so it is not surprising that there is some overlap here. Also, there is most likely some pixel mixing occurring, and this could account for the crossover of these classes. Grass was best separated using bands 91 and 96 which have center wavelengths of 1190 and 1264 nm, which is in the near infrared region of the spectrum. If the image was taken at another time of the year, these bands would most likely change.

**Table 2. Best Bands and ROC $A_z$ values.**

| CLASS | Az | BANDS | CLASS | Az | BANDS | CLASS | Az | BANDS |
|---|---|---|---|---|---|---|---|---|
| **Water** | 0.972 | 66, 131 | **Buildings** | 0.997 | 8, 11 | **Trees** | 0.833 | 62 |
| **Shadow** | 0.943 | 118 | **Paths** | 0.808 | 2, 3, 10 | **Grass** | 0.936 | 91, 96 |

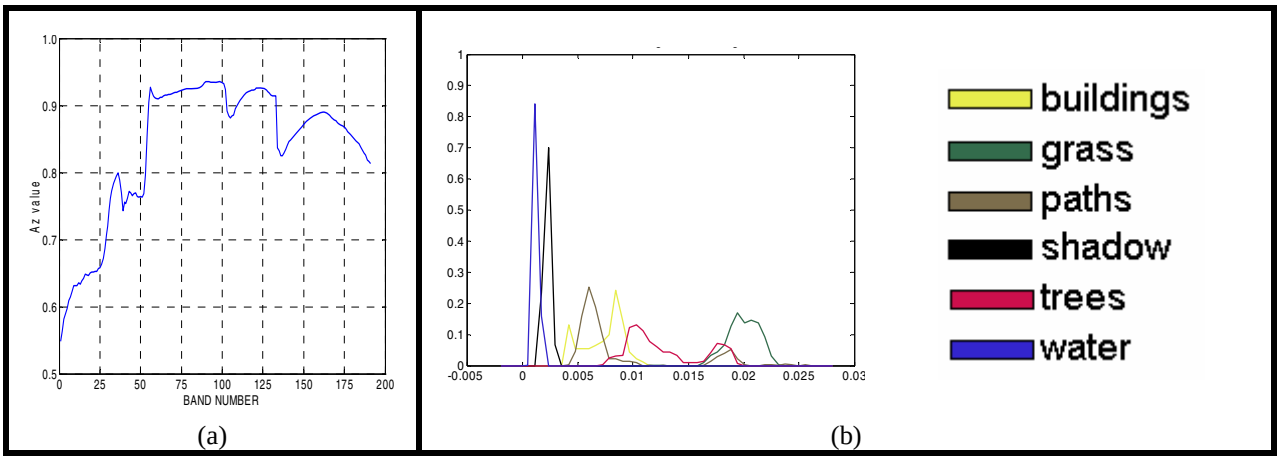


**Figure 2.** FLDA weighting coefficients applied to grass signatures. (a) Plots of ROC $A_Z$ values vs. band number from best bands analysis. (b) Plot of PDF of each class after projection into the FLDA feature space by using the FLDA weight coefficients.

After determining the best bands, the resulting matrices were examined and the scaling parameters were selected in order to produce a reasonable speed function, since each method had a different procedure for creating $\Sigma$. If the parameter was set too low or too high, then the image would be severely over or under-segmented. The weighting constants were experimentally determined: $\alpha_k$ is 0.20, 0.05, 2.00, 0.02, and 0.50 for $k = 1 \ldots 5$, respectively.

Figure 3(a) shows the original hyperspectral image in false color. Figure 3(b) and 3(c) shows the locations of testing regions, which are color coded based on the endmember, superimposed on and grayscale version of the image, and the color scheme for each endmember, respectively. Figure 3(d)-(i) shows the segmentation results (thematic map) for methods 1 – 6, respectively. From Figure 3, it appears that the test area for buildings is too large, and this will show as poor producer's accuracies for this class.

A visual inspection of Figure 3 shows that all methods did a fairly good job. Method 3 was the only one that correctly segmented the water in the upper left hand side of the image. Method 6 appears to have over segmented grass over trees. Method 6 picked up small trees in the upper right hand corner that methods 1-5 missed. Method 6 had sporadic building pixels, which was prevented by the strong discriminant function used in methods 1-5. Method 2 slightly over segmented the water boundary (the Potomac) near the bottom of the triangular area in the top left-hand corner of the image. Method 6 did not find as many shadows as the other methods. A quantitative comparison of the results is shown in Table 3 and Figure 4. Table 3 shows the confusion matrices for each method, and the user's, producer's and overall accuracies are shown in Figure 4(a)–(c), respectively. In general, shadows and buildings had some confusion in all methods. Method 6 confused trees with buildings and paths. The results for methods 1-4 are quite similar, based on user's, producer's and overall accuracies.

Overall, water and buildings were segmented with the most user's accuracy. All user's accuracies were above 90%. The producer's accuracies for buildings are misleading, since the ground truth data overestimated the building size. Methods 1-4 provided the best overall results, with method 5 nearly as good, and method 6 much worse. This could be due to using the particular three bands chosen, although methods 5 and 6 used the same bands. The striking similarities between methods 1-4 may indicate that the similarity function has provided near optimal results, and that the discriminator functions were very critical because they stopped the level set propagation for all of these methods.

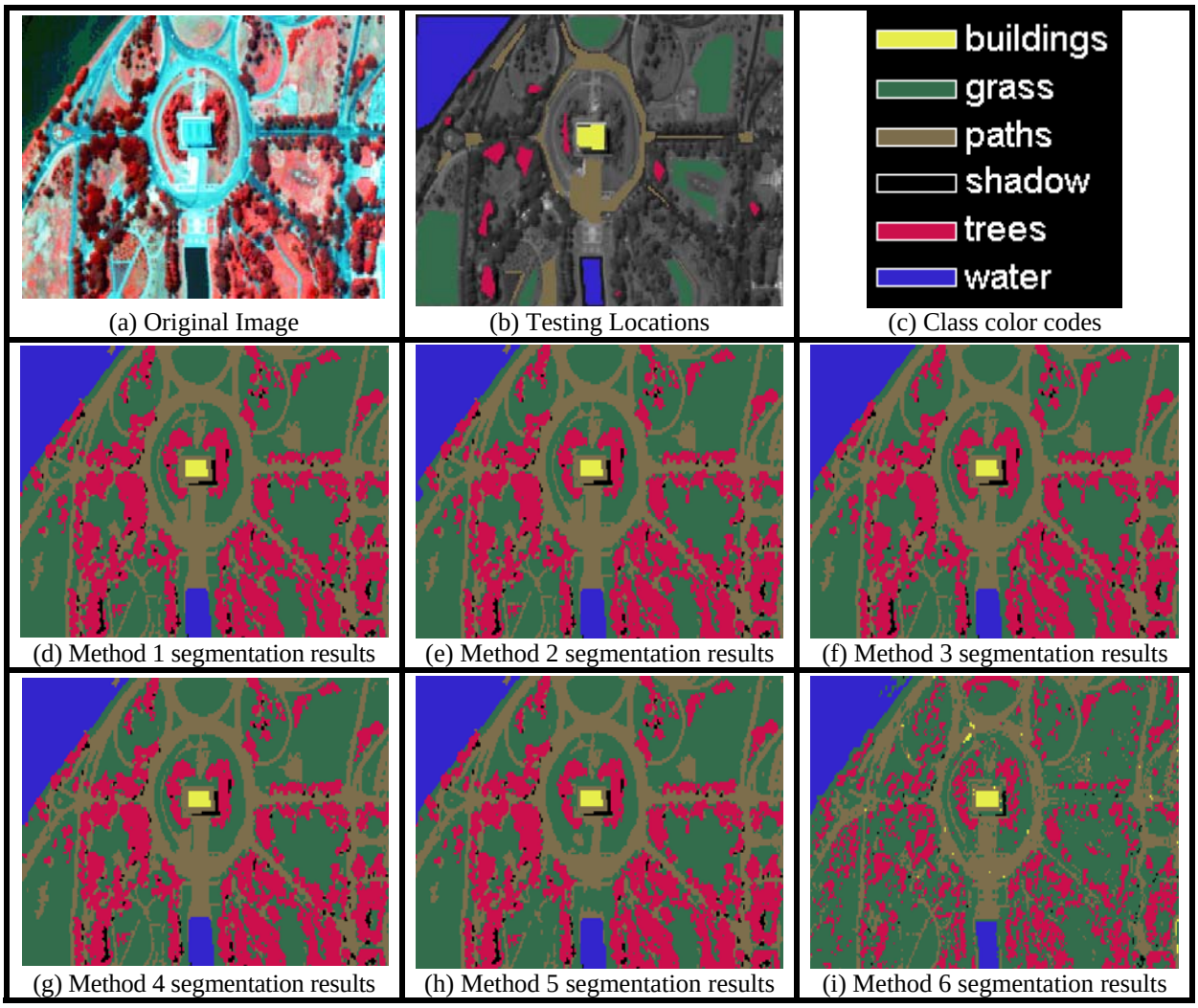


(a) Original Image (b) Testing Locations (c) Class color codes

(d) Method 1 segmentation results (e) Method 2 segmentation results (f) Method 3 segmentation results

(g) Method 4 segmentation results (h) Method 5 segmentation results (i) Method 6 segmentation results

**Figure 3.** (a) Original image (false color RGB). (b) Black and white image with testing areas overlaid in color. (c) Color codes for the classes. (d) – (i) are the segmentation results for methods 1-6, respectively.

## CONCLUSIONS

The overall classification accuracies for the four proposed methods were very good and outperformed methods 5 and 6. Methods 3 and 4 seemed to be the best performing. The importance of the discriminator functions is critical, and these were not modified from the previous research. Also, it was surprising how well methods 1-4 performed with the low $A_Z$ values for paths and trees, as well as the small number of bands selected by the band selection algorithm. Methods 1-4 had accuracies on par or better than with many of the segmentation schemes discussed earlier.

Future work could include: (i) a more automated method of generating the discriminator functions; (i) automated selection of proper weighting parameters for the spectral similarity functions; (iii) investigating non-linear methods for band selection, such as KDA or SVM based methods; and (iv) applying the method to other images of different dimensionalities and in other settings (i.e. a rural image).

**Table 3. Confusion Matrices.**

| | W | S | B | P | T | G |
|---|---|---|---|---|---|---|
| **W** | **94** | 0 | 0 | 0 | 0 | 0 |
| **S** | 0 | **2640** | 187 | 0 | 5 | 0 |
| **B** | 75 | 68 | **1487** | 0 | 4 | 9 |
| **P** | 0 | 0 | 0 | **22** | 1 | 0 |
| **T** | 0 | 0 | 13 | 0 | **432** | 0 |
| **G** | 0 | 0 | 0 | 0 | 4 | **1759** |

(a) Method 1.

| | W | S | B | P | T | G |
|---|---|---|---|---|---|---|
| **W** | **94** | 0 | 0 | 0 | 0 | 0 |
| **S** | 0 | **2640** | 181 | 0 | 5 | 0 |
| **B** | 75 | 68 | **1493** | 0 | 4 | 9 |
| **P** | 0 | 0 | 0 | **22** | 1 | 0 |
| **T** | 0 | 13 | 0 | 0 | **432** | 0 |
| **G** | 0 | 0 | 0 | 0 | 4 | **1759** |

(b) Method 2.

| | W | S | B | P | T | G |
|---|---|---|---|---|---|---|
| **W** | **94** | 0 | 0 | 0 | 0 | 0 |
| **S** | 0 | **2640** | 204 | 0 | 0 | 9 |
| **B** | 75 | 68 | **1470** | 0 | 0 | 0 |
| **P** | 0 | 0 | 0 | **22** | 1 | 0 |
| **T** | 0 | 0 | 13 | 0 | **433** | 0 |
| **G** | 0 | 0 | 0 | 0 | 3 | **1768** |

(c) Method 3.

| | W | S | B | P | T | G |
|---|---|---|---|---|---|---|
| **W** | **94** | 0 | 0 | 0 | 0 | 0 |
| **S** | 0 | **2640** | 187 | 0 | 5 | 0 |
| **B** | 75 | 68 | **1487** | 0 | 4 | 9 |
| **P** | 0 | 0 | 0 | **22** | 1 | 0 |
| **T** | 0 | 13 | 0 | 0 | **432** | 0 |
| **G** | 0 | 0 | 0 | 0 | 4 | **1759** |

(d) Method 4.

| | W | S | B | P | T | G |
|---|---|---|---|---|---|---|
| **W** | **94** | 0 | 0 | 0 | 0 | 0 |
| **S** | 0 | **2681** | 290 | 0 | 5 | 0 |
| **B** | 75 | 29 | **1384** | 0 | 4 | 9 |
| **P** | 0 | 0 | 0 | **22** | 1 | 0 |
| **T** | 0 | 0 | 11 | 0 | **434** | 0 |
| **G** | 0 | 0 | 0 | 0 | 2 | **1759** |

(e) Method 5.

| | W | S | B | P | T | G |
|---|---|---|---|---|---|---|
| **W** | **101** | 0 | 8 | 0 | 0 | 0 |
| **S** | 2 | **2412** | 299 | 12 | 194 | 36 |
| **B** | 66 | 51 | **1316** | 0 | 0 | 0 |
| **P** | 0 | 0 | 0 | **10** | 0 | 0 |
| **T** | 0 | 0 | 258 | 51 | **252** | 0 |
| **G** | 0 | 0 | 0 | 0 | 0 | **1732** |

(f) Method 6.

**CLASS LEGEND:** **W**=Water **S**=Shadow **B**=Buildings **P**=Paths **T**=Trees **G**=Grass

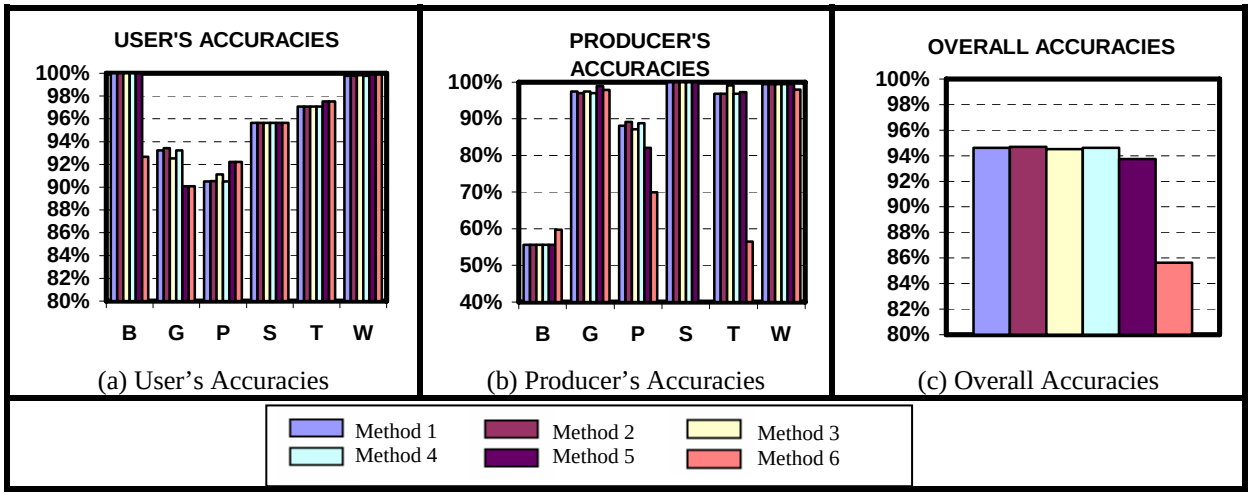


(a) User's Accuracies (b) Producer's Accuracies (c) Overall Accuracies

**Figure 4.** Graphs of accuracies. (a) User's accuracies. (b) Producer's accuracies. (c) Overall accuracies.

## ACKNOWLEDGEMENT

The authors would like to acknowledge the National Science Foundation for providing J. Ball's research fellowship and Ian Mitchell for providing a robust and well documented level set toolbox for Matlab. J. Ball would like to acknowledge Dr. Lori Bruce for providing FLDA and ROC $A_Z$ calculation code in Matlab.

## REFERENCES


Ball, J.E., and L.M. Bruce (2005). "Level set segmentation of remotely sensed hyperspectral images." *Proceedings of the 2005 IEEE International Geoscience and Remote Sensing Symposium*, 8:5638–5642.

Brox, T., and J. Weickert, (2004). "Level set based image segmentation with multiple regions." in *Pattern Recognition*, Rasmussen, C.-E., H. Bulthoff, H., M. Giese, M. and B. Scholkopf , eds., Springer.

Bruce, L.M., C.H. Koger, and J. Li (2002). "Dimensionality reduction of hyperspectral data using discrete wavelet transform feature extraction." *IEEE Transactions on Geoscience and Remote Sensing*, 40(10):2331–2338.

Camps-Valls, G., and L. Bruzzone (2005). "Kernel-based methods for hyperspectral image classification." *IEEE Transactions on Geoscience and Remote Sensing*, 43(6):1351–1362.

Chang, C.-I, Q. Du, T.-L. Sun, and M.L.G. Althouse (1999). " A joint band prioritization and band-decorrelation approach to band selection for hyperspectral image classification." *IEEE Transactions on Geoscience and Remote Sensing*, 37(6):2631–2641.

Cheriyadat, A. and L.M. Bruce (2003). "Why principal component analysis is not an appropriate feature extraction method for hyperspectral data." *Proceedings of the 2003 IEEE International Geoscience and Remote Sensing Symposium*, 6:3420–3422.

Congalton, R.G. (1998). *Assessing the accuracy of remotely sensed data: principles and practices*, CRC Press.

Dell'Acqua, F., P. Gamba, and P. Prevedini (2000). Level-set based extraction and tracking of meteorological objects in satellite images. *Proceedings of the IEEE International Geoscience and Remote Sensing Symposium*, 2:627–629.

Du, H., H. Qi, X. Wang, R. Ramanath, W.E. Snyder (2003). "Band selection using independent component analysis for hyperspectral image processing." *Proceedings of the 32nd Applied Imagery Pattern Recognition Workshop*, 1:93–98.

Du, Q. (2003). "Band selection and its impact on target detection and classification in hyperspectral image analysis." *2003 IEEE Workshop on Advances in Techniques for Analysis of Remotely Sensed Data*, 1:374–377.

Duda, R.O., P. Hart, and D. Stork (2001). *Pattern Classification*, 2nd ed., Wiley Interscience.

Fukanaga, K. (1990). *Introduction to Statistical Pattern Recognition*, 2nd ed., Academic Press.

Gamba, P., F. Dell'Acqua, and P. Prevedini (2000). "Level-set based extraction and tracking of meteorological objects in satellite images", *Proceedings of the 2000 IEEE International Geoscience and Remote Sensing Symposium*, 2:627–629.

Gu, Y., Y. Zhang, and J. Zhang (2002). "A kernel based nonlinear subspace projection method for reduction of hyperspectral image dimensionality." *Proceedings of the 2002 International Conference on Image Processing*, 2:II-357 – II-360.

Halldorsson, G.H., J.A. Benediktsson, and J.R. Sveinsson (2004). "Source based feature extraction for support vector machines in hyperspectral classification." *Proceedings of the 2004 IEEE International Geoscience and Remote Sensing Symposium*, 1:536–539.

Hanley, J.A., and B.J. McNeil, "The meaning and use of the area under a receiver operating characteristics (ROC) curve." *Diagnostic Radiology*, 143:29–36.

Harper, P, and R.B. Reilly (2000).Color based video segmentation using level sets. *Proceedings of the International Conference on Image Processing*, 3:480–483.

Li, J., L.M. Bruce, and A. Mathur (2002), "Wavelet transform for dimensionality reduction in hyperspectral linear unmixing." *Proceedings of the 2002 IEEE International Geoscience and Remote Sensing Symposium*, 6:3513–3515.

Kaewpijit, S., J. Le Moigne, and T. El-Ghazawi (2003). "Automatic reduction of hyperspectral imagery using wavelet spectral analysis." *IEEE Transactions on Geoscience and Remote Sensing*, 41(4):863–871.

Keaton, T. and J. Brokish (2002). A level set method for the extraction of roads from multispectral imagery. *Proceedings of the Applied Imagery Pattern Recognition Workshop*, 1:141–147.

Krissian, K., J. Ellsmere, K. Vosburgh, R. Kikinis, and C.-F. Westin (2003). Multiscale segmentation of the aorta in 3D ultrasound images. *Proceedings of the Engineering in Medicine and Biology Society*, 1:638–641.

Kuybeda, O., A. Kagan, and Y. Lumer (2004). "Determining hyperspectral data-intrinsic dimensionality via a modified Gram-Schmidt process." Proceedings. 2004 23rd IEEE Convention of Electrical and Electronics Engineers in Israel, 1:380–383.

Landgrebe, D.A. (2003). *Signal theory methods in multispectral remote sensing*. Wiley.

Lee, C.P., W. Snyder, and C. Wang (2005). "Supervised Multispectral Image Segmentation using Active Contours." *Proceedings of the 2005 IEEE International Conference on Robotics and Automation*, 1:4242–4247.

Lillesand, T.M., R.W. Kiefer, and J.W. Chipman (2003). *Remote Sensing and Image Interpretation*, Wiley.

Mitchell, I. (2005). “A Toolbox of level set methods, Version 1.1 beta, March 6, 2005.” http://www.cs.ubc.ca/~mitchell/ToolboxLS /index.html.

Osher, S. and N. Paragios, eds. (2003). *Geometric level set methods in imaging, vision and computer graphics*, Springer.

Riedmann, M., and E.J. Milton (2003). “Supervised band selection for optimal use of data from airborne hyperspectral sensors.” *Proceedings of the 2003 IEEE International Geoscience and Remote Sensing Symposium*, 3:1770–1772.

Sethian, J., *Level set methods and fast marching methods*, 2nd ed. (1999). Cambridge University Press.

Sumengen, B., B.S. Manjunath, and C. Kenney (2001). Image segmentation using curve evolution. *Conference Record of the Thirty-Fifth Asilomar Conference on Signals, Systems and Computers*, 2:1141–1145.

Suri, J.S. and S. Laxminarayan, eds. (2002). *PDE & level sets: algorithmic approaches to static and motion imagery*. Kluwer Academic.

Tu, T.-M., C.-H. Chen, J.-L. Wu, and C.-I Chang, “A fast two-stage classification method for high-dimensional remote sensing data.” *IEEE Transactions on Geoscience and Remote Sensing*, 36(1):182–191.

Venkataraman, S., L.M. Bruce, A. Cheriyadat, and A. Mathur (2005). “Hyperspectral dimensionality reduction via localized discriminant bases.” *Proceedings of the 2005 IEEE International Geoscience and Remote Sensing Symposium*, 2: 1245–1248.

Welling, M. (2005), “Fisher Linear Discriminant Analysis.” Lecture notes, University of Toronto, Canada. www.ics.uci.edu/~welling/classnotes/papers_class/Fisher-LDA.pdf.

_____, AVIRIS home page. http://aviris.jpl.nasa.gov/.

_____, Band specifications for the HYDICE Washington D.C. Mall Image provided on the compact disk with “Signal theory methods in multispectral remote sensing.” http://www.lars.purdue.edu/home/image_data/hydice_dc_wavelengths.html.

_____, Leica Geosystems Inc. (2005). ERDAS Image Software Suite Information website. http:gis.leica-geosystems.com/product_units/geographic_imaging/.